Compromised perfusion in femoral head in normal rats: distinctive perfusion MRI evidence of contrast washout delay

[1]Y-X J WANG, MMed, PhD, [1]J F GRIFFITH, FRCR, [1]M DENG, MMed, [2,4]H T MA, PhD, [3]Y-F ZHANG, MMed, PhD, [5]S-X YAN, MD and [1]A T AHUJA, FRCR

[1]*Department of Imaging and Interventional Radiology, The Chinese University of Hong Kong, Prince of Wales Hospital, Shatin, Hong Kong, China,* [2]*Jockey Club Centre for Osteoporosis Care and Control, The Chinese University of Hong Kong, Prince of Wales Hospital, Shatin, Hong Kong, China,* [3]*Department of Medicine and Therapeutics, The Chinese University of Hong Kong, Prince of Wales Hospital, Shatin, Hong Kong, China,* [4]*Department of Electronic and Information Engineering, Harbin Institute of Technology Shenzhen Graduate School, Shenzhen, China, and* [5]*Department of Radiation Oncology, the First Affiliated Hospital, College of Medicine, Zhejiang University, Hangzhou, China*

Objectives: The femoral head is prone to osteonecrosis. This study investigated dynamic contrast-enhanced (DCE) MRI contrast washout features of the femoral head and compared the data with data from other bony compartments in normal rats.
Methods: 7-month-old Wistar rats were used. DCE MRI of the right hip ($n=18$), right knee ($n=12$) and lumbar spine ($n=10$) was performed after an intravenous bolus injection of Gd-DOTA (0.3 mmol kg^{-1}). Temporal resolution was 0.6 s for hip and spine, and 0.3 s for knee. The total scan duration was 8 min for hip and spine, and 4.5 min for knee. The regions of interest for enhancement measurement included femoral head, proximal femoral diaphysis, distal femoral diaphysis and epiphysis, proximal tibial epiphysis and diaphysis, and lumbar vertebrae L1–5.
Results: Femoral head showed no enhancement signal decay during the DCE MRI period, while all other bony compartments showed a contrast washin phase followed by a contrast washout phase. In the knee joint, the contrast washout of the proximal tibia diaphysis was slower that of other bony compartments of the knee.
Conclusion: Based on the evidence of delayed contrast washout, this study showed that blood perfusion in the femoral head could be compromised in normal rats.

Received 13 December 2010
Revised 21 March 2011
Accepted 4 May 2011

DOI: 10.1259/bjr/25916692

Clinical studies have shown that the femoral head has a poorer blood supply compared with the femoral neck and femoral shaft [1, 2]. MRI-derived perfusion indices of maximum enhancement and enhancement slope for the femoral head were only about one-fifth to one-quarter of those for the femoral shaft in healthy elderly male and female subjects [1]. Because of the absence of an effective collateral circulation, the femoral head is at an especially high risk of ischaemic injury [3]. Osteonecrosis of the femoral head may be idiopathic or secondary to numerous diseases. Bone perfusion can affect bone metabolism and microdamage repair. Osteonecrosis can have early vascular components that change underlying bone perfusion in the affected bone and joint, and contribute to the clinical cascade of disease [4]. Relatively mild haemodynamic impairment, which may not necessarily compromise other sites, has the potential to cause osteonecrosis of the femoral head [1, 5, 6]. In animals, osteonecrosis of the femoral head is sporadically encountered in dogs [7]. Perthes disease-like necrosis of the femoral head and neck occurs in some breeds of small dogs [7]. Osteonecrosis of the femoral head is also seen in spontaneously hypertensive rats [8–10]. Recently it was reported that delayed washout in dynamic contrast-enhanced (DCE) MRI suggests compromised blood perfusion in the tissue, including blood stasis or outflow obstruction [11]. It was also reported that delayed contrast washout could be seen in sites of bone marrow oedema, osteoarthritis and avascular osteonecrosis [11]. This study investigated DCE MRI contrast washout features of the femoral head in normal mature rats. The results from the femoral head were compared with the data from proximal and distal femoral diaphysis, distal femoral epiphysis, proximal tibial epiphysis and diaphysis, and lumbar vertebral bodies.

Methods and materials

The experimental protocol was approved by the animal experiment ethics committee of the Chinese University of Hong Kong. 7-month-old mature Wistar rats were used in this study. The animals were housed 2–3 animals per stainless steel cage at 22 °C under a 12-hour light, 12-hour dark cycle while receiving a standard commercial rat chow and water diet *ad libitum.* For MRI examinations, the rats were anaesthetised using a combination of xylazine (10 mg kg^{-1}) and ketamine (90 mg kg^{-1}).

Address correspondence to: Dr Yi-Xiang Wang, Department of Imaging and Interventional Radiology, Prince of Wales Hospital, The Chinese University of Hong Kong, Shatin, NT, Hong Kong, China.
E-mail: yixiang_wang@cuhk.edu.hk
This study is supported by a direct grant for research from the Chinese University of Hong Kong (2041501), by GRF of Hong Kong SAR (project no. 464508) and partially by a grant from the Research Grants Council of the Hong Kong SAR (project no. SEG_CUHK02).

DCE MRI of the right hip (n=18) was performed on a 1.5 T clinical whole-body imaging system (Intera® NT; Philips Healthcare, Best, Netherlands). DCE MRI of the right knee (n=12) and spine (n=10) was performed on a 3 T clinical whole-body imaging system (Achieva™; Philips Healthcare). Before MRI, the rat tail vein was cannulated with a 24 G heparinised catheter (Introcan Safety; B Braun Medical Inc., Bethlehem, PA). For MRI of the hip, the rat was positioned supinely in a custom-made cradle. A surface coil with a diameter of 4.7 cm was placed under the hip as the radiofrequency (RF) receiver and the body volume coil was used as the RF transmitter. After the scout scan, a plane through the femoral head, femoral neck and femoral shaft of the right side femur was prescribed by three-point planscan tool. For MRI of knee, a single loop coil with a diameter of 2.3 cm (finger coil) was used as the RF receiver and the body volume coil was used as the RF transmitter. A platform described by Wang [12] was used to hold the finger coil and rats. Animals were placed on a Perspex platform with one hind leg extending through the RF coil and the knee centred in it. To prevent motion, the animal's right paw was secured to a secondary lower platform. After the scout scan, a central sagittal plane of the knee was prescribed. For MRI of the spine, a custom-made quadrature volume RF coil of 7-cm internal diameter was used as signal transmitter and receiver. Rats were placed in the coil supine, and a central sagittal plane was prescribed. For all MRI examinations, T_1 weighted anatomical images were obtained prior to DCE scans.

For the hip, the following dynamic MR scan series was obtained: gradient echo sequence, repetition time (TR)=4 ms, echo time (TE)=1.4 ms, flip angle=15°, slice thickness=5 mm, acquisition resolution=0.625 × 0.625 mm, temporal resolution=0.6 s per acquisition, average=1. For the knee, the following dynamic MR scan series was obtained: gradient echo sequence, TR=5.4 ms, TE=2.3 ms, flip angle=12°, slice thickness=2 mm, acquisition resolution=0.63 × 0.83 mm, temporal resolution=0.3 s per acquisition, average=1. For lumbar spine, the following dynamic MR scan series was obtained: gradient echo sequence, TR=5.4 ms, TE=2.3 ms, flip angle=12°, slice thickness=2 mm, acquisition resolution=0.63 × 0.63 mm, temporal resolution=0.6 s per acquisition, average=1. MRI contrast agent was Gd-DOTA. A dose of 0.3 mmol kg^{-1} (0.15 ml for a 250-g rat) was hand-injected after initial baseline 60-image acquisitions as quick bolus and followed by a flush of 0.5 ml normal saline. The DCE MRI scan duration was 8 min for hip and spine examinations, and 4.5 min for knee examinations.

Dynamic MRI images were processed in a radiological workstation (Workspace; Philips Medical Systems, Best, Netherlands). Regions of interest (ROIs) were drawn over the cancellous part of (1) femoral head (FH), (2) femoral neck (FN), (3) proximal femoral diaphysis (PFD), (4) distal femoral diaphysis (DFD), (5) distal femoral epiphysis (DFE), (6) proximal tibial epiphysis (PTE), (7) proximal tibial diaphysis (PTD) and (8) lumbar vertebrae L1–L5. The signal enhancement over time was recorded. For quantitative analysis, as all the lumbar vertebrae in each rat showed very similar enhancement pattern, DCE MRI data of vertebra L3 were used. The small size of FN made it prone to partial volume effect and consequently quantitative analysis was not carried out.

To characterise the contrast washout phase of DCE curve, maximum washout amplitude (*MaxOut*), washout rate (*Rout*), and washout time (*Tout*) were calculated. To standardise the data obtained from DCE MRI on different anatomical locations, only the initial 4.5 min of data were used. Each DCE signal curve was first processed by a self-designed digital low-pass filter to remove high-frequency noise, followed by normalisation with baseline signal: $S'(t)=[S(t)-S_0]/S_0$, where S(t) was the original signal intensity changing with time after contrast injection and S_0 was the signal intensity before contract injection. Based on the pre-processed signal S′(t), *MaxOut* was defined as the signal change from the initial peak enhancement to the signal end, where a positive value indicated a signal decrease and a negative value indicated a signal increase. *Tout* (in minutes) was the time duration from the initial peak enhancement to the signal end. *Rout* (in percentage per min) was the value of *MaxOut* divided by *Tout*, reflecting the speed of signal change after the initial peak enhancement. First and second differential signals of S′(t) were employed to identify the initial peak. For the DCE signal curves with a

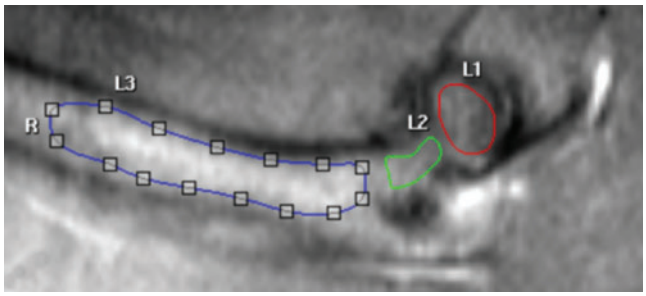

(a)

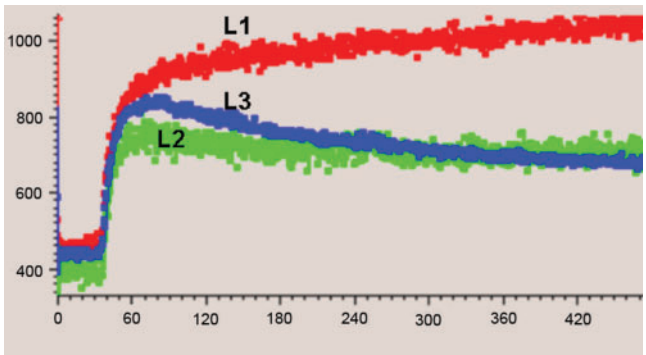

(b)

Figure 1. (a) T_1 weighted anatomical image depicting femoral head (L1), femoral neck (L2) and proximal femoral diaphysis (L3). (b) Dynamic contrast-enhanced MRI time–signal intensity curve (*y*-axis: signal intensity in arbitrary units; *x*-axis: time in seconds). In the proximal femoral diaphysis, signal intensity curve drops after peak enhancement in proximal femoral shaft (L3, blue line). In contrast, after a rapid rising phase the time–signal intensity curve in the femoral head continues to increase slowly, and no washout is observed 440 s post-contrast injection (L1, red line). The time–signal intensity curve of femoral neck is close to femoral shaft although the washout curve is flatter than that of the proximal femoral diaphysis. R, right (femur).

signal decay during the washout, the initial peak time point was detected by finding out the cross-zero point in the first differential signal, which also indicates the maximum enhancement. For those DCE signal curves that continued to increase during the whole DCE examination duration, the initial peak was defined as the most changed point of the curve changing trend. This was detected by the cross-zero point in the second differential signal, and also confirmed by visual inspection of the DCE signal curve. All signal processing was realised by programming in Matlab® (v. R2009a; Mathworks Inc., Natick, MA).

Data were expressed as mean ± standard deviation. Wilcoxon's signed-rank test was used for paired comparison between FH and PFD. One-way analysis of variance and *post hoc* tests for multiple comparisons were used for the four components in the knee. All statistical analyses were performed using SPSS version 14.0 (SPSS Inc, Chicago, IL). A p-value of <0.05 was considered statistically significant. No quantitative comparison was made between the joints as these data were acquired using different scanners and RF coils.

Results

Satisfactory DCE MRI data were obtained for all FH, PFD and lumbar spine. For the knee joint, owing to the limitation of longitudinal length of the ''finger coil'', it was difficult to place the four compartments (*i.e.* DFD, DFE, PTE and PTD) always in the centre of the coil. Those DCE data with unsatisfactory positioning were discarded for quantitative analysis, so available numbers of DFD, DFE, PTE and PTD were 11, 12, 11 and 7, respectively.

It was observed that with all 18 FH data, after the initial fast contrast washin, there was no subsquent signal decay (*i.e.* no contrast washout observed until the end of the DCE scan). Instead, in 16 FHs there was a second further slower contrast signal increase phase (Figure 1), and in two cases, after the initial fast washin phase, the contrast signal curve was flat. The enhancement pattern of the femoral neck was closer to that of the femoral shaft, although the washout curve tended to be flatter (Figure 1). On the other hand, all the PFD showed a fast contrast washin phase followed by a contrast washout phase (Figure 1). In the knee joint, all four compartments of DFD, DFE, PTE and PTD showed a fast contrast washin phase followed by a contrast washout phase (Figure 2). All the vertebrae showed a similar enhancement pattern, with a fast contrast washin phase followed by a contrast washout phase (Figure 3). The quantitative data of *MaxOut*, *Rout* and *Tout* are shown in Table 1.

Taking the absolute value for comparison, it was noted that in the hip joint the mean values of *MaxOut* and *Rout* were higher in PFD than in FH (both $p<0.001$), indicating that the magnitude of post-contrast signal change and its speed were greater in the PFD than in FH. The mean *Tout* value of FH was smaller than that of PFD ($p<0.001$), indicating that the enhancement signal in the FH reached initial peak later than in the PFD. In the knee joint, there was no difference in mean *Tout* for its four components, indicating that contrast enhancement reached initial peak at the same speed in these four compartments. In the knee joint, it was noted that PTD had a smaller mean *MaxOut* and mean *Rout* (both $p<0.05$) than the other three compartments.

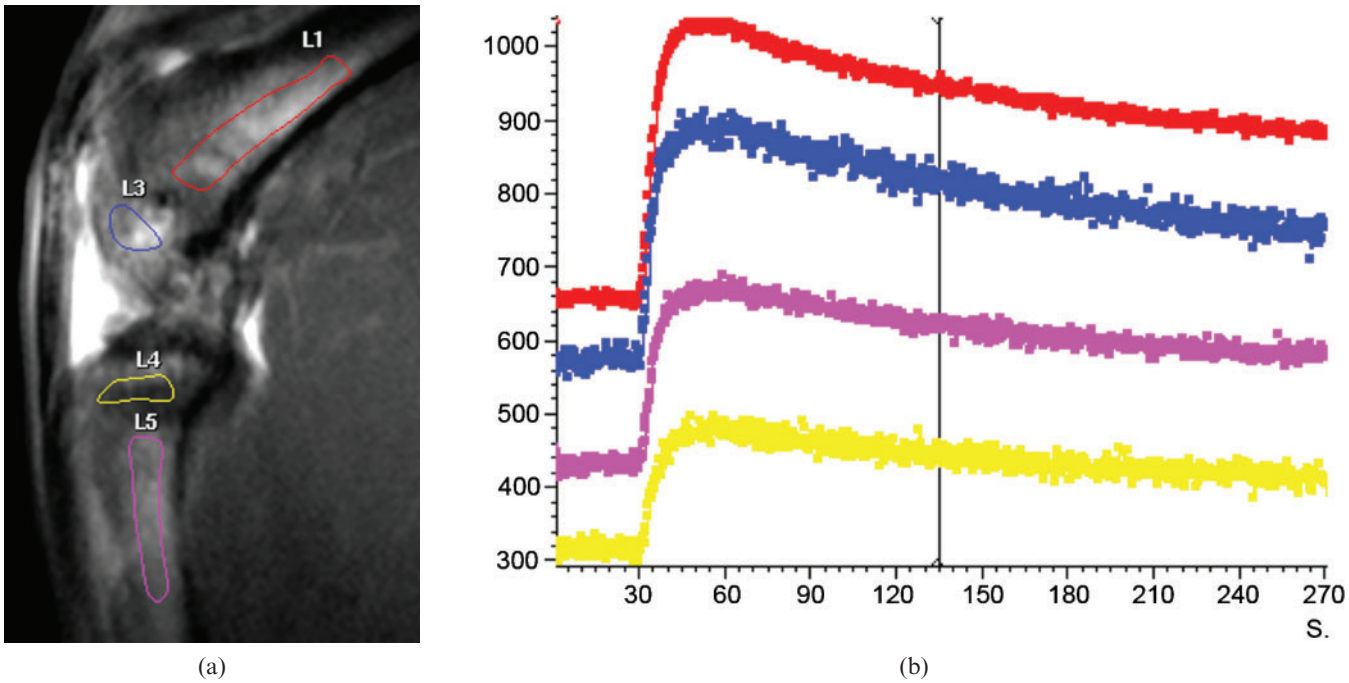

(a) (b)

Figure 2. (a) MRI sagittal view of right knee of a rat. T_1 weighted anatomical image depicting distal femoral diaphysis (L1), distal femoral epiphysis (L3), proximal tibial epiphysis (L4) and proximal tibial diaphysis (L5). (b) Dynamic contrast-enhanced MRI time–signal intensity curves. After bolus injection of Gd-DOTA, all four regions have a rapid rising phase. The time–signal intensity curves decrease after peak enhancement.

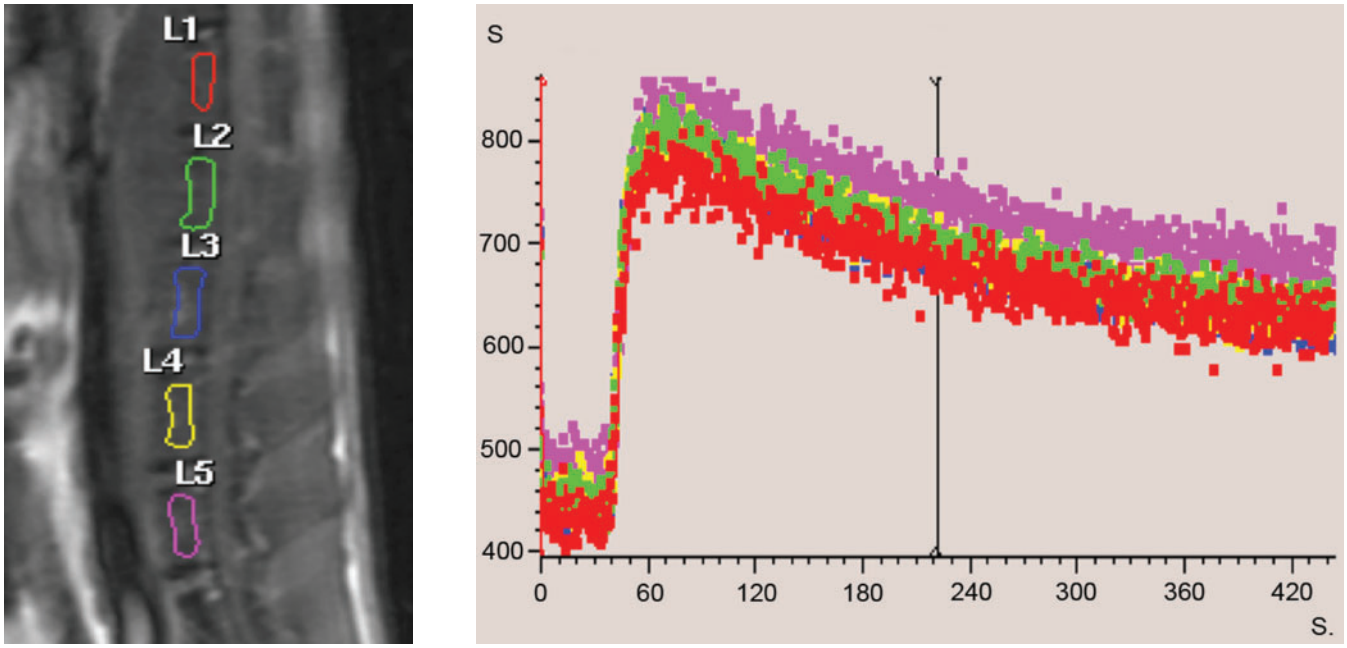

(a) (b)

Figure 3. (a) MRI sagittal view of lumbar spine of a rat. ROIs were drawn over vertebrae L1–L5. (b) Dynamic contrast-enhanced MRI time–signal intensity curves. After bolus injection of Gd-DOTA, all five vertebrae show similar enhancement pattern, with a rapid contrast washin phase followed by a contrast washout phase.

Discussion

Osteonecrosis of the femoral head is sporadically seen in animals [7]. The cause of this osteonecrosis is still under investigation. Osteonecrosis of the femoral head has been studied in 6-week-old to 8-month-old spontaneously hypertensive rats [8–10]. It was reported that the route of the lateral epiphyseal arteries, the main nutrient suppliers, differs in spontaneously hypertensive rats from that in other rat strains in that the vessels abruptly decrease in diameter at their entry sites into the ossific nucleus of the epiphysis. Stenosis or obstruction of the lumen of these arteries develops. In parallel with the most severely affected parts, the ensuing ischaemia induces osteonecrosis at the lateral epiphyseal facets of the femoral heads. In the meantime, it is understood that hydrostatic pressure of intra-articular fluids plays a pivotal role in regulating the femoral head's blood supply, the blood flow decreasing with increasing intra-articular pressure.

The complex nature of osteonecrosis can be due to vascular impediment, microembolic events, adipocytic hypertrophy and lipid-incurred osteocytic death, alone or in combination, playing aetiopathogenic roles of unequal magnitudes under different circumstances [13]. In human subjects, it is reported that changes in bone perfusion are related to many entities, including bone marrow oedema, osteoarthritis and osteonecrosis [11]. In osteoarthritis and osteonecrosis, early signs may manifest as local changes in the fluid dynamics of the subchondral bone. Bone marrow oedema is an imaging marker of increased intra-osseous pressure and changes in blood flow. Increases in intra-osseous pressure and decreases in oxygen concentrations are seen in osteoarthritis and osteonecrosis, and have been related to bone pain [14]. Conventional contrast studies have demonstrated venous engorgement and stasis associated with intra-osseous hypertension in osteoarthritis of the hip [14]. Similar elevations of intra-osseous pressure were found in patients with osteoarthritis of the knee [15].

Table 1. Quantitative washout results of bony compartments in hip, knee and spine

	Hip		Knee				Spine
Washout parameters	FH (n=18)	PFD (n=18)	DFD (n=11)	DFE (n=12)	PTE (n=11)	PTD (n=7)	Vertebra L3 (n=10)
Mean *MaxOut*	−17.5±12.7%	50.9±18.8%[a]	19.4±7.9%	16.9±8.5%	20.0±8.6%	9.5±7.5%[b]	36.5±8.7%
Mean *Rout*	−5.3±4.8%	14.1±5.0%[a]	5.8±2.1%	5.1±2.5%	5.8±2.3%	2.1±2.2%[b]	11.6±2.7%
Mean *Tout*	3.2±0.5	3.6±0.2[a]	3.3±0.5	3.4±0.5	3.3±0.5	3.2±0.6	3.2±0.1

FH, femoral head; PFD, proximal femoral diaphysis; DFD, distal femoral diaphysis; DFE, distal femoral epiphysis; PTE, proximal tibial epiphysis; PTD, proximal tibial diaphysis; *MaxOut*, maximum washout; *Rout*, washout rate; *Tout*, time of washout (min); *n*, number of joints used for analysis.

Negative values of FH indicate MR signal increase. Positive values of PFD, DFD, DFE, PTE, PTD and vertebra L3 indicate MR signal decrease.

[a] $p<0.001$.

[b] $p<0.05$.

Osteotomy of the proximal femur reduces intra-osseous pressure and pain in patients with osteoarthritis of the hip [14].

MR signal changes observed via DCE MRI can be due to a combination of, among other things, capillary permeability, tissue blood perfusion and interstitial tissue pressure [11, 16–18]. In the DCE MRI study, washout is related to the back-flow of contrast agent from interstitial space to the bloodstream and the elimination of contrast agent from the body via the kidneys. For the first time, our *in vivo* MRI observation suggested that even in normal mature Wistar rats the perfusion of FH demonstrated a lack of washout phase within 8 min, possibly due to the specific fluid dynamics of the subchondral bone in FH. Femoral and tibial epiphysis of the knee, proximal tibial diaphysis and lumbar vertebrae showed a contrast washin phase followed by a contrast washout phase, indicating that the delayed washout in FH was not due to its being an epiphysis. This result will be relevant for understanding the physiology and pathophysiology of hip joint diseases in animal models. It can be seen that the perfusion characteristics of the femoral neck lay between those of FH and PFD, and were closer to PFD than to FH (Figure 1). This feature of femoral neck blood flow dynamics in rats is similar to the results from a recent DCE MRI study of human subjects [1]. Another interesting aspect observed in this study is that PTD had a smaller *MaxOut* and *Rout* than the other compartments of the knee. Its physiological importance and histological base remain to be further explored. In human subjects, it is well known that tibial fractures typically take a long time to heal, and are often associated with impaired healing, including delayed union or non-union [19].

One limitation of our study is that clear washout of FH was not observed. It can be expected that if DCE MRI examination is carried out for long enough, a contrast signal-decreasing washout phase of femoral head will eventually be seen. In our study, long DCE scan was prohibited owing to limited access to the machine time of clinical scanners. However, in three randomly selected rats, a second hip joint MRI was performed 24 h after the initial MRI, and it was noticed that the contrast agent had completely washed out from the femoral head by that time. Additionally, because the absolute value of contrast washout parameters can be influenced by the MRI scan duration [20], studies to further clarify the washout features of FH in rats will be valuable. Pharmacokinetic modelling was not used in this study as a suitable arterial input function could not be obtained. The small structures in the rat joints suffered from low signal-to-noise ratio. This caused difficulties in T_1 mapping. Another limitation is that the DCE MRI of the rat hip was carried out with a 1.5 T scanner, while that of rat knee and spine was carried out with a 3 T scanner. The 1.5 T scanner was decommissioned during the course of this study. We expect the change of scanner not to have affected the results in this study. It is conceivable that there will be some similarities, and also some dissimilarities, between femoral head physiology of rats and human subjects. Further studies on DCE MRI characteristics of the human femoral head will be valuable.

In conclusion, our *in vivo* MRI observation suggested for the first time that even in normal mature Wistar rats the perfusion of FH is compromised compared with other bony sites. The histological and physiological mechanism of the observed MRI phenomenon remains to be further investigated.

References

1. Wang YX, Griffith JF, Kwok AW, Leung JC, Yeung DK, Ahuja AT, et al. Reduced bone perfusion in proximal femur of subjects with decreased bone mineral density preferentially affects the femoral neck. Bone 2009;45:711–15.
2. Kubo T, Kimori K, Nakamura F, Inoue S, Fujioka M, Ueshima K, et al. Blood flow and blood volume in the femoral heads of healthy adults according to age: measurement with positron emission tomography (PET). Ann Nucl Med 2001;15:231–5.
3. Downey DJ, Simkin PA, Lanzer WL, Matsen FA III. Hydraulic resistance: a measure of vascular outflow obstruction in osteonecrosis. J Orthop Res 1988;6:272–8.
4. Cheras PA, Freemont AJ, Sikorski JM. Intraosseous thrombosis in ischemic necrosis of bone and osteoarthritis. Osteoarthr Cartil 1993;1:219–32.
5. Yamamoto T, Bullough PG. The role of Subchondral insufficiency fracture in rapid destruction of the hip joint: a preliminary report. Arthritis Rheum 2000;43:2423–7.
6. Nakamura F, Fujioka M, Takahashi KA, Ueshima K, Arai Y, Imahori Y, et al. Evaluation of the hemodynamics of the femoral head compared with the ilium, femoral neck and femoral intertrochanteric region in healthy adults: measurement with positron emission tomography (PET). Ann Nucl Med 2005;19:549–55.
7. Boss JH, Misselevich I. Osteonecrosis of the Femoral Head of Laboratory Animals: The Lessons Learned from a Comparative Study of Osteonecrosis in Man and Experimental Animals. Vet Pathol 2003;40:345–54.
8. Oda J, Hirano T, Iwasaki K, Majima R. Vascular occlusion and cartilage disorders in osteonecrosis of the femoral head in rats. Int Orthop 1996;20:185–9.
9. Hirano T, Iwasaki K, Sagara K, Nishimura Y, Kumashiro T. Necrosis of the femoral head in growing rats. Occlusion of lateral epiphyseal vessels. Acta Orthop Scand 1989;60:407–10.
10. Iwasaki K, Hirano T, Sagara K, Nishimura Y. Idiopathic necrosis of the femoral epiphyseal nucleus in rats. Clin Orthop Relat Res 1992;277:31–40.
11. Lee JH, Dyke JP, Ballon D, Ciombor DM, Tung G, Aaron RK. Assessment of bone perfusion with contrast-enhanced magnetic resonance imaging. Orthop Clin North Am 2009;40:249–57.
12. Wang YX. In vivo magnetic resonance imaging of animal models of knee osteoarthritis. Lab Anim 2008;42:246–64.
13. Cruess RL. Osteonecrosis of bone. Current concepts as to etiology and pathogenesis. Clin Orthop 1986;208:30–9.
14. Arnoldi CC, Linderholm H, Mussbichler H. Venous engorgement and intraosseous hypertension in osteoarthritis of the hip. J Bone Joint Surg Br 1972;54:409–21.
15. Arnoldi CC, Lemperg K, Linderholm H. Intraosseous hypertension and pain in the knee. J Bone Joint Surg Br 1975;57:360–3.
16. Wang YX, Zhang YF, Griffith JF, Zhou H, Yeung DK, Kwok TC, et al. Vertebral blood perfusion reduction associated with vertebral bone mineral density reduction: a dynamic contrast-enhanced MRI study in a rat orchiectomy model. J Magn Reson Imaging 2008;28:1515–18.
17. Reddick WE, June S, Taylor JS, Fletcher BD. Dynamic MR imaging (DEMRI) of microcirculation in bone sarcoma. J Magn Reson Imaging 1999;10:277–85.

18. Taylor JS, Wilburn E, Reddick WE. Evolution from empirical dynamic contrastenhanced magnetic resonance imaging to pharmacokinetic MRI. Adv Drug Deliv Rev 2000;41:91–110.
19. Dahabreh Z, Calori GM, Kanakaris NK, Nikolaou VS, Giannoudis PV. A cost analysis of treatment of tibial fracture nonunion by bone grafting or bone morphogenetic protein-7. Int Orthop 2009;33:1407–14.
20. Wang YX, Zhou H, Griffith JF, Zhang YF, Yeung DK, Ahuja AT. An in-vivo MRI technique for measurement of rat lumbar vertebral body blood perfusion. Lab Anim 2009; 43:261–5.